Symmetry-Based Transformable and Foldable Plate Structures

Valentina Beatini
Department of Architecture,
Abdullah Gul University,
Sumer Campus,
Kayseri 38280, Turkey
e-mail: valentina.beatini@agu.edu.tr

This paper presents a novel family of modular flat-foldable rigid plate structures composed by assemblies of 4R-linkages. First, in the field of foldable plates, the proposed system is characterized by being not only foldable but also transformable: the slope of one module over the other is capable of changing not only magnitude but also sign. This transformable behavior extends the range of application of foldable plates from simply larger–smaller configurations to substantially different configurations and usages. The transformable curve is obtained by means of symmetry operations on the spherical length of links. For each module, three configurations can be designed. Various examples are illustrated. [DOI: 10.1115/1.4036648]

Keywords: assemblies of spherical linkages, Grashof's criterion, foldable structures, origami, multistable mechanisms

1 Introduction

This paper presents a novel family of modular plate mechanisms, characterized by being not only foldable but also transformable. The term transformable here refers to the slope of one module over the preceding one, which can change not only magnitude but also sign. Thus, the curve traced by the plates during motion can move, for example, from a concave profile to a convex one and vice versa.

The mechanism has one degree-of-freedom, DOF; it is flat-foldable and composed of rigid plates.

The construction of the modules and their assemblies is based on symmetry operations. One may divide the existing foldable plate structures into two families: the ones based on symmetry constraints and the ones which are not. Roughly speaking, while the first are assemblies of modules, which fold flat and generally have mobility one, the second leave more freedom in the design of the profile described by the mechanism. The proposed system is based on symmetry constraints, but fewer than in common, existing systems. Noteworthy, fewer constraints are employed here that change the sign of the curvature described by the mechanism; thus, it can substantially change its shape.

The importance of symmetry for the design of spherical linkages composed by four revolute joints and four links, 4*R*-linkages, had been recently highlighted in Refs. [1] and [2]. The idea emerges from Kokotsakis [3]. He studied quadrangular plates (quads) whose inside vertexes are shared by four plates; he demonstrated that, if the spherical length of links is constant, then they fold continuously from a flat-folded state to another, perpendicular one. Given the constant spherical length of links, such quad plates are arranged into doubly symmetrical 4*R*-spherical linkages.

The so called *egg-box* and Miura-like tessellations are highly studied Kokotsakis meshes [4–7]. Also, symmetrical arrangements of groups of generic 4*R*-spherical linkages have been proposed [8]. As discussed in this paper, the equal spherical length of the links makes them capable of reaching two flat-folded states.

Wider possibilities have been disclosed by Watanabe and Kawaguchi [9]; he discards symmetry and focuses on generic foldable quad plates, still arranged in 4*R*-linkages. However, where assemblies are concerned, the spherical links tend to interfere with each other; the design of links capable of reaching a flat-folded state becomes a recursive process, which may not find a solution, and which is usually neglected from calculation [10].

Flat-foldability is even more difficult to achieve when linkages have more than four links [11,12]. In such cases, the mechanism may also exhibit more than one DOF [13,14].

Foldable plate structures are usually employed in packaging, as well to create space structures, architectural envelopes, design furniture, and medical equipment. Mobility one and flat-foldability are generally considered desirable requirements because they make the control easier and the structure efficiently packable. Meanwhile, their constraints limit the range of shapes and surfaces that the mechanism can approximate. The mechanism presented here has just one completely flat-folded state and one partially flat-folded state. Indeed, if only one fully flat-folded state is acceptable, then, as detailed in the paper, it can be achieved with reduced symmetry and by using plates of different shape.

Actually, the possibility of combing different plates with a prescribed procedure has been investigated also in Ref. [15], although in that case the aim was to decrease the span of the structure in the fully flat folded state. In the study presented here, the freedom given by the reduced constraints is used to improve the range of shapes that the mechanism can approximate and in particular to change the sign of curvature described by the mechanism during motion.

The substantially different shapes that the very same mechanism can approximate while folding may open new possible uses. Indeed, one can think not of simply smaller and larger configurations but of even inverted shapes. Each transformable–foldable module can be assembled in order to reach three desired slopes over the preceding one during motions. The derived ribs can be further assembled into surfaces.

Section 2 discusses the model and its constraints with reference to the unit sphere. Section 3 exemplifies the mechanism's design. Under the constraints expressed in Sec. 3.1, the slope of one module over the preceding one reaches during motion three desired values, as exemplified in Sec. 3.2, and different modules can be combined in order to obtain curves whose shape changes over time, Sec. 3.3. Dimensioning the plates allows reproducing desired curves, but it also may have consequences on the mobility and interference of plates during motion, as discussed in Sec. 4. The overall achievements, drawbacks, and possible further developments are discussed in the conclusions.

Contributed by the Mechanisms and Robotics Committee of ASME for publication in the JOURNAL OF MECHANICAL DESIGN. Manuscript received June 21, 2016; final manuscript received March 29, 2017; published online May 18, 2017. Assoc. Editor: Dar-Zen Chen.

2 The Model

2.1 The Role of Symmetry in 4*R*-Spherical Linkage Assemblies. In order to describe the mechanism and its possible generalizations, a brief focus on symmetry is presented. Any assembly of plates by means of revolute joints is a spherical linkage; especially, when four plates meet at a vertex, a 4*R*-linkage is obtained. The linkage shares many properties with its planar counterpart [16]. In particular, the Grashof's criterion in its traditional form defines the ability of links to rotate based on their reciprocal linear length. It states that any stand-alone 4*R*-linkage, whose sequential links have linear length *a*, *a*, *a*, *a* or *a*, *b*, *a*, *b,* has two perpendicular states in which all links are collinear. If the considered length is the spherical one, the criterion holds also for spherical linkages [17]. Thus, the linkages have two flat-folded states when the sum of the spherical length of either two adjacent links is equal to the sum of the spherical length of the other two. There are two alternative ways to achieve such spherical linkages by means of plate structures. Linkages composing the *egg-box* and the Miura tiling have links of spherical length *a*, *a*, *a*, *a*. At each vertex, the planar angles of plates are, respectively, equal or supplementary. Linkages whose ordered links have spherical length *a*, *b*, *a*, *b* underlie the Huffman tessellation and its variations [18,19].

Within a 4*R*-linkage, links whose lengths are a_i, a_i, a_i, a_i, create a cyclic symmetry of order 4. Continuing the parallelism with planar linkages, one can consider linear assemblies of planar 4*R*-linkages, subjected to cyclic symmetry of order 4, but with variable length a_i from linkage i to linkage $i+n$. If the two links shared by any two adjacent linkages are straight, Fig. 1(*a*), geometry imposes that the angles σ at the left and at the right of the shared joint are equal. In addition, since the linkages are symmetrical around the transversal, parallel axes, σ is constant throughout the assembly: the linkages become longitudinally colinear at once. Meanwhile, the longitudinal plane of symmetry within each linkage imposes that also the two remaining angles are equal. Therefore, while the angle σ reaches its max, the transversal angle tends to zero everywhere; eventually, all the linkages become transversally colinear simultaneously. Similarly, plates whose spherical links at each vertex create a cyclic symmetry of order 4, can be freely assembled in a row and their foldability is unaffected by the length of links, either spherical or linear. Two such linkages are depicted with different color in Fig. 1(*b*). Each link shared by the adjacent linkages now lies in one plane; as before, it follows that the dihedral angles τ at the left and at the right of the shared joint are equal. Again, the transversal symmetry of the linkages, together with the planarity of each plate, imposes that the dihedral angles along the longitudinal plane are constant throughout the assembly, $\tau_i = k, \forall i$, and that all linkages reach a longitudinal collinear state at once. Looking at Fig. 1(*c*), the plates in this starting position are longitudinally flat-folded. Meanwhile, because of the longitudinal symmetry within each linkage, when τ is max, all linkages are transversally collinear. In this end position, plates are transversally flat-folded.

Many foldable plates proposed in literature are implicitly based on these properties [20–22]. The only constraint is that spherical links are not a quarter of a great circle. It is

$$a_{i;j} \neq \frac{N\pi r}{2}, \forall i \tag{1}$$

where subscripts identify the vertexes of the 2D grid, centers of the spherical linkages, while superscripts identify the two possibly different links within each linkage. If this condition is neglected, the spherical representation would be improper, half, or an entire great circle, and the mechanism would be in a stacked configuration.

The mechanism presented in this paper breaks the sequence of doubly foldable spherical linkages and thus the sequence of constant dihedral angles between them.

2.2 The Minimal Transformable–Foldable Mechanism. A minimal transformable–foldable mechanism is depicted in Fig. 2 together with its spherical representation. As usual, spherical lengths are indicated with Latin letters while the corresponding planar angles are now introduced in the plate representation and indicated with Greek letters.

As mentioned earlier, the structure is composed of two doubly symmetrical 4*R*-spherical linkages and a mixed 4*R*-linkage in between. Again, different color tones identify each linkage while different saturation of colors indicates links of different spherical length. The module is composed of a doubly symmetrical linkage and half of the mixed linkage. Modules are identified by two numbers *s*;*t* where *s* is the sequential module along *i* and *t* is the sequential module along *j*. Angles are defined by subscripts *i*;*j*, which refer to the vertexes of the plate structure and by superscript *s*, which identifies the module moving along vertexes *i*;*j*, to $i+n$;*j*. Since spherical linkages do not change along the transversal direction *j*, no superscript *t* is applied in the definitions of angles.

The two doubly symmetrical linkages are centered at vertexes 1;1 and 3;1 and are composed, respectively, by links of equal

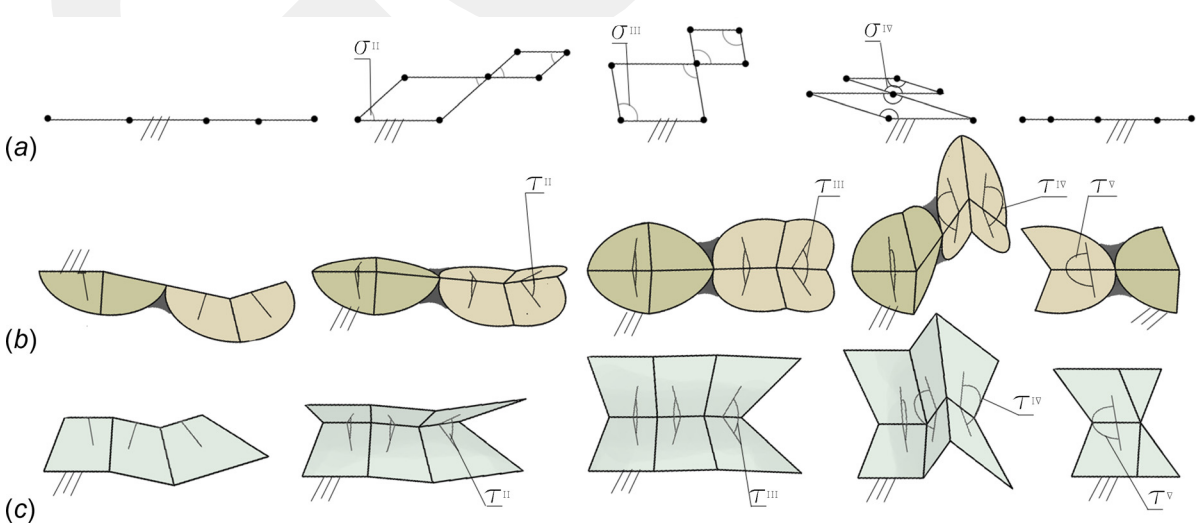

Fig. 1 Linear assemblies of doubly symmetrical 4*R*-linkages: (*a*) planar linkages, (*b*) spherical linkages, and (*c*) the plate structure correspondent to (*b*)

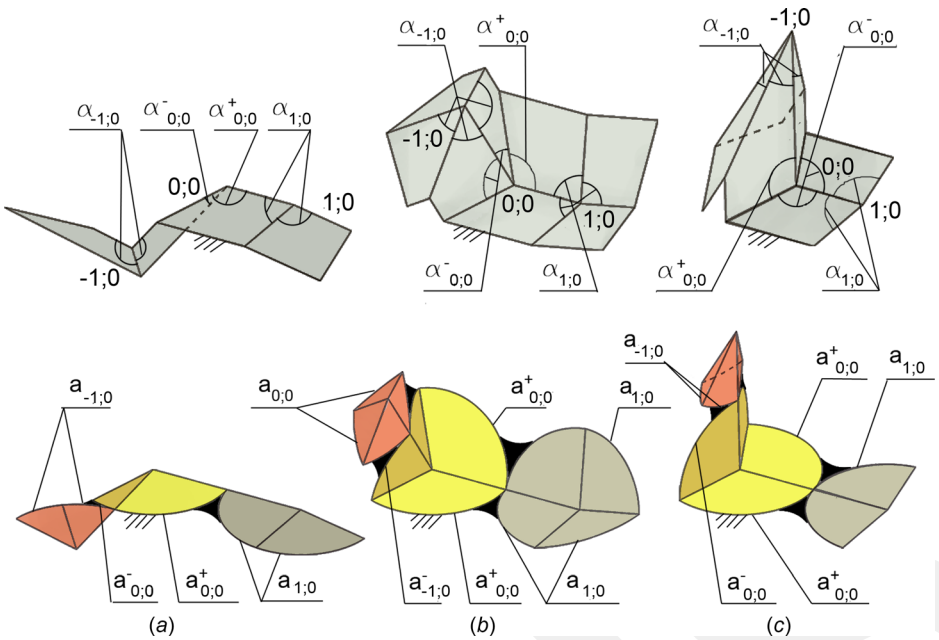

Fig. 2 A minimal transformable mechanism where $a^1_{2;1}<a^2_{2;1}$ and its spherical representation during motion: (*a*) starting position: fully flat-folded state, (*b*) generic unfolded position, and (*c*) end position: partially flat-folded state

spherical length $a^1_{1;1}$ and $a^2_{3;1}$. The links of the mixed linkage, centered at vertex 2;1, have spherical length

$$a^1_{2;1} \neq a^2_{2;1} \tag{2}$$

Within each 4*R*-linkage, one may total the spherical length of links below and above the (longitudinal) line of symmetry and find they are equal. The conditions discussed in Sec. 2.1 for longitudinal flat foldability still hold and the linkages can flat fold at once along the common line of symmetry.

The existence of a second, perpendicular flat-folded state is guaranteed if, within each linkage, the sum of the spherical length of links to the right and to the left of the transversal axis is equal. Theoretically, both the end linkages can reach a second, perpendicular flat-folded state. However, the mixed linkage, centered in 2;1, does not have transversal symmetry. Its shorter links become collinear while the other two remain unfolded; therefore, just the end linkage connected to the shorter central links becomes collinear. In the plate structure, the plates corresponding to the collinear spherical links become transversally flat-folded.

As detailed in Sec. 3.1, the relative spherical length of links can be set so that the angle between adjacent modules reaches any three desired values during motion.

2.3 Linear Assemblies. A linear assembly is illustrated in Fig. 3. Looking at Fig. 3(*b*), as before, the 4*R*-linkages are centered at the vertexes of the plate structure, labeled *i*;*j*, and are represented with a different color tone. Different saturation of colors indicates links of different spherical length. Each module spans from the center of a mixed linkage to the center of the successive one, and it comprises a number of doubly symmetrical linkages in between. Although the number of doubly symmetrical linkages from one module to the other may differ, this does not alter the transmission angle within their plates. The transmission angle changes from one module to the other.

In addition to the constraints of the minimal mechanism previously discussed, within ribs it is

$$a^s_{i;j} - a^{s+1}_{i;j} = K_1, \forall s \tag{3}$$

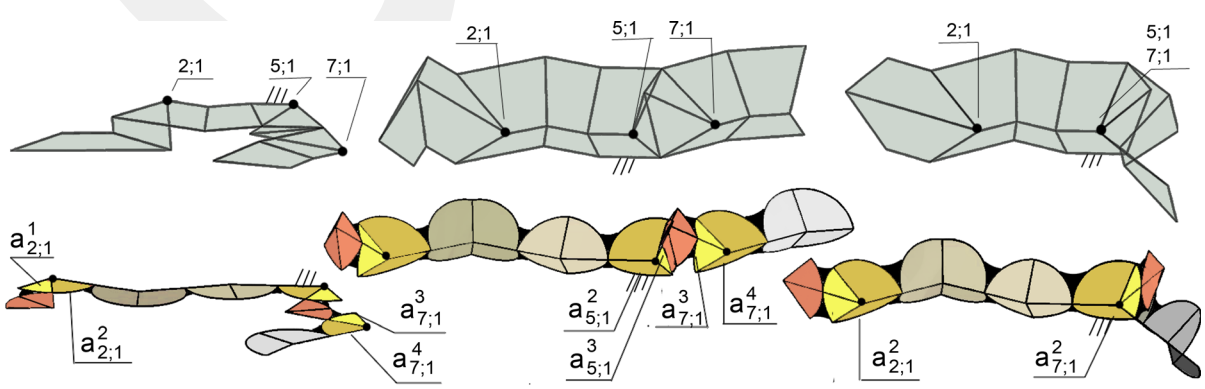

Fig. 3 (*a*) Folding phases of a linear assembly. The centers of mixed linkages are indicated. (*b*) Spherical representation of the same assembly. Different color tones refer to different 4*R*-linkages (see figure online for color).

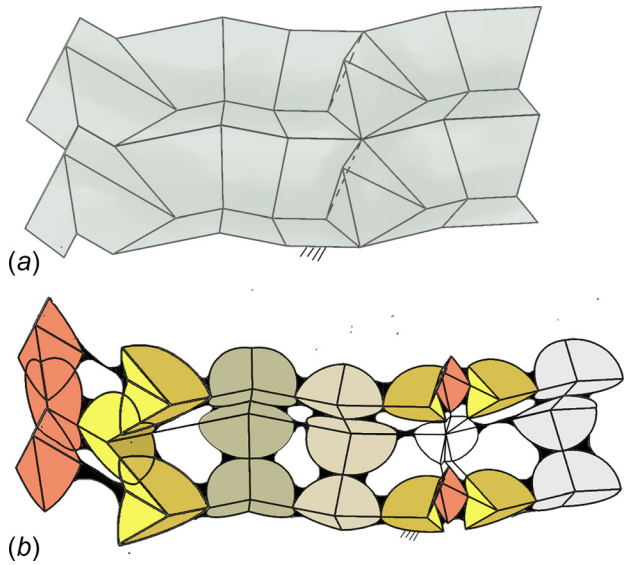

Fig. 4 Generic unfolded position of a spatial assembly: (*a*) the plate structure and (*b*) the spherical links

where s is the sequential index identifying the module along the i direction. Equation (3) ensures that the variation of transmission angle provided by the mixed linkage is kept constant throughout the assembly. Since the transmission angle between the other, doubly symmetrical linkages is constant throughout the surface by construction, it is ensured, therefore, that all modules are able to fold harmoniously and to reach the designed folded states at the same time. The other necessary condition to provide a harmonious folding is to keep mobility equal to one. As discussed in Sec. 4.2, this always happens in the case of quadrangular plates.

2.4 Spatial Assemblies. Modules can be added in two directions to create surfaces, Fig. 4. In Fig. 4(*b*), the composing 4*R*-linkages are highlighted. While most of the plates are quads, at the right, there are four interconnected triangular plates. Their spherical links obey the same rules already discussed. As detailed in Sec. 4.2, they are surrounded by 4*R*-linkages composed only by quadrangular plates; thus, they do not increase mobility.

The linkages can be freely added along the transversal direction until they have equal spherical images

$$a^s_{i;j} = k_2, \ \forall j, \text{ in case of quadrangular plates} \tag{4a}$$

$$a^s_{i;j} = a^s_{i;j+2} = k_3, \ \forall j, \text{ in case of triangular plates} \tag{4b}$$

This quite limiting constraint ensures that the plates fold harmoniously: the spherical span of the linkages varies longitudinally; however, at any folding phase, it is constant along the transversal direction. Accordingly, the quad plates have parallel longitudinal sides along the transversal direction, Fig. 4(*a*).

3 Design

3.1 Three-Position Synthesis. As mentioned in the introduction, the transformable and foldable behavior is achieved through the reciprocal inclination of modules linearly assembled. Each module $s+1;t$ can be designed to reach three desired degrees of curvature $(\omega^{s,s+1})$, $(\omega^{s,s+1})'$, and $(\omega^{s,s+1})''$ during motion over the preceding one, $s;t$. With reference to Fig. 5, the following parameters are introduced.

$\vartheta^s_{i;j}$ is the angle between sides belonging to modules $s;t$, $t=\forall$, $\overline{(i;j)(i+1;j)}$ or $\overline{(i-1;j)(i;j)}$, and the plane through vertexes $i;j-z_0$, $i;j$, and $i;j+z_1$, $z_0, z_1 \in Z$; $\tau^s_{i;j}$ is the angle between side $\overline{(i;j)(i;j+1)}$ and the plane through vertexes $i-z_2;j$, $i;j$, and $i+z_3;j$ $z_2, z_3 \in Z$.

Again, since spherical linkages do not change along the transversal direction j, no superscript t is applied in the definitions of angles.

Considering three modules, module $s;t$, which diagonally spans from vertex $(i_0;j_0)$ to $(i_0+2;\ j_0+2)$, module $s+1;\ t$, which diagonally spans from $(i_0+2;\ j_0)$, to $(i_0+4;\ j_0+2)$, and module $s;\ t+1$, which diagonally spans from $(i_0+2;\ j_0)$, to $(i_0+2;\ j_0+4)$, the following angles are introduced.

$\omega^{s,s+1;t} = \omega^{s,s+1}$ is the degree of curvature of two adjacent modules $s;\ t$ plus $s+1;\ t$, defined as the total angle between the vw

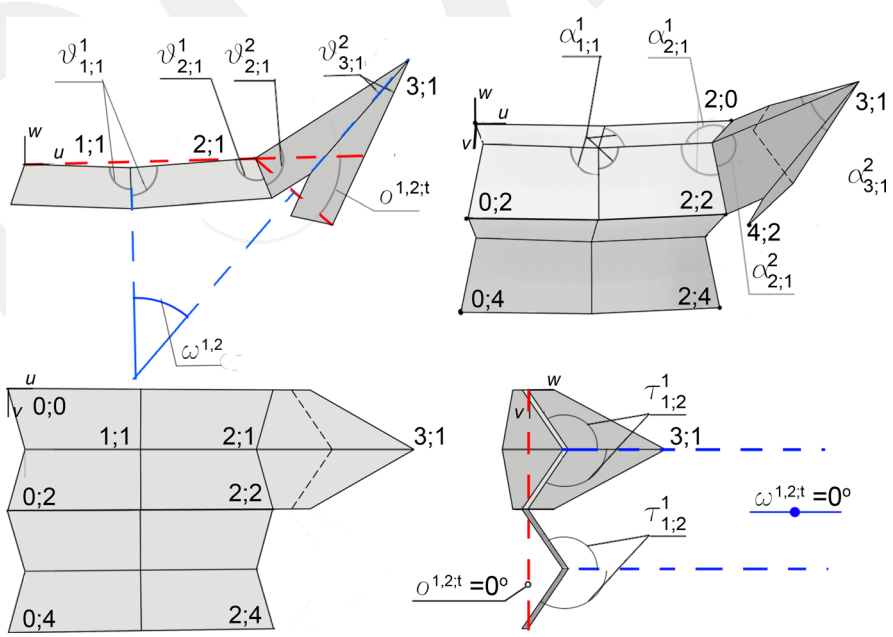

Fig. 5 The plate structure, planar angles $\alpha^s_{i;j}$, fold angles $\vartheta^s_{i;j}$ and $\tau^s_{i;j}$ between sides of plates at vertexes *i*, *j*, degree of curvature $\omega^{s,s+1}$, and inclination angles $o^{s,s+1;t}$ and $o^{s;t,t+1}$ defining the slope of modules

plane bisector of module s; t, defined by vertexes $(i_0+1;\ j_0)$, $(i_0+1;\ j_0+1)$ and $(i_0+1;\ j_0+2)$, and the vw plane bisector of module $s+1$; t, defined by vertexes $(i_0+3;\ j_0)$, $(i_0+3;\ j_0+1)$, and $(i_0+3;\ j_0+2)$ $\omega^{s;t,t+1}$ is the degree of curvature of two adjacent modules s;t plus s; $t+1$, defined as the total angle between the uw plane bisector of module s;t, defined by vertexes $(i_0;\ j_0+1)$, $(i_0+1;\ j_0+1)$, and $(i_0+2;\ j_0+1)$, and the uw plane bisector of module s; $t+1$, defined by vertexes $(i_0;\ j_0+3)$, $(i_0+1;\ j_0+3)$, and $(i_0+2;\ j_0+3)$.

It is noted that, spherical links being simply translated along j, it is by construction

$$\omega^{s;t,t+1} = 0\,\text{deg}, \forall t \tag{5}$$

Additionally, the slope between modules is defined as:

$o^{s,s+1;t}$ is the inclination angle of module $s+1$; t over s; t, measured in anticlockwise direction, from line $\overline{(i_0+4;j_0)(i_0+2;j_0)}$ to line $\overline{(i_0;j_0)(i_0+2;j_0)}$, $o^{s;t,t+1}$ is the inclination angle of module s;$t+1$ over s;t, measured in anticlockwise direction, from line $\overline{(i_0;j_0+4)(i_0;j_0+2)}$ to line $\overline{(i_0;j_0)(i_0;j_0+2)}$.

In the case that the doubly symmetrical 4R-linkages are created by symmetrical plates, plates within each module being all equal, angles $\omega^{s,s+1}$ and $o^{s,s+1;t}$ have the same value, and so $o^{s;t,t+1} = \omega^{s;t,t+1} = 0\,\text{deg}$.

The degree of curvature between two modules can be calculated based only on angular relationships. Between modules where planar angles within the doubly symmetrical linkages are in the form $\alpha^s_{i;j} = \alpha^{s+1}_{i;j}$, $\alpha \neq 0\,\text{deg}$, (egg-box tiling), the degree of curvature $\omega^{s,s+1;t}$ reads

$$\sin(\omega^{s,s+1}) = -\sin\left(\sum_{i=n_0}^{n_1}\vartheta^s_{i;j} + \sum_{i=n_1}^{n_2}\vartheta^{s+1}_{i;j}\right),\ \text{for}\ \alpha^s_{n_1;j} > 90\,\text{deg},\ \alpha^{s+1}_{n_1;j} < 90\,\text{deg} \tag{6a}$$

$$\sin(\omega^{s,s+1}) = \sin\left(\sum_{i=n_0}^{n_1}\vartheta^s_{i;j} - \sum_{i=n_1}^{n_2}\vartheta^{s+1}_{i;j}\right),\ \text{for}\ \alpha^s_{n_1;j} > 90\,\text{deg},\ \alpha^{s+1}_{n_1;j} < 90\,\text{deg} \tag{6b}$$

The degree of curvature between modules where the same planar angles are in the form $\alpha^s_{i;j} = \pi - \alpha^{s+1}_{i;j}$, $\alpha \neq 0\,\text{deg}$, (Miura-like tiling) reads

$$\sin(\omega^{s,s+1}) = \sin\left(\sum_{i=n_0}^{n_{1-1}}\vartheta^s_{i;j} - \vartheta^s_{n_1;j} + \sum_{i=n_1}^{n_2}\vartheta^{s+1}_{i;j}\right),\ \text{for}\ \alpha^s_{i;j} < 90\,\text{deg},\ \alpha^{s+1}_{i;j} > 90\,\text{deg} \tag{6c}$$

$$\sin(\omega^{s,s+1}) = -\sin\left(\sum_{i=n_0}^{n_{1-1}}\vartheta^s_{i;j} - \vartheta^s_{n_1;j} + \sum_{i=n_1}^{n_2}\vartheta^{s+1}_{i;j}\right),\ \text{for}\ \alpha^s_{i;j} > 90\,\text{deg},\ \alpha^{s+1}_{i;j} > 90\,\text{deg} \tag{6d}$$

At each target configuration, the constraints discussed in Sec. 2 need to be expressed with reference to the longitudinal and transversal projections of the plates in their middle planes.

Equations (1) and (2) read

$$\sin(\alpha^s_{i;j}) \neq 1, \forall i \tag{7}$$

$$\sin(\alpha^s_{i;j}) \neq \sin(\alpha^{s+1}_{i;j}) \tag{8}$$

The symmetry constraints read

$$\frac{\tan(\tau^s_{i;j})}{\sin(\vartheta^s_{i;j})} = \frac{\tan(\tau^s_{i+1;j})}{\sin(\vartheta^s_{i+1;j})}, \forall j \tag{9a}$$

$$\frac{\sin(\tau^s_{i;j})}{\sin(\alpha^s_{i;j})} = \frac{\sin(\tau^s_{i+1;j})}{\sin(\alpha^s_{i+1;j})}, \forall j \tag{9b}$$

with $\vartheta, \tau \neq 0\,\text{deg}$.

In addition, by construction it is

$$\cos(\alpha^s_{i;j}) = \cos(\tau^s_{i;j})\cos(\vartheta^s_{i;j}) \tag{10}$$

At any position, the minimal mechanism is fully defined by the seven angles between plates plus the four planar angles describing the plates. Three desired configurations C, C', and C'' can be designed. They are obtained by setting the desired increasing or decreasing degrees of curvature, $\omega^{s,s+1}$, $(\omega^{s,s+1})'$, $(\omega^{s,s+1})''$, and

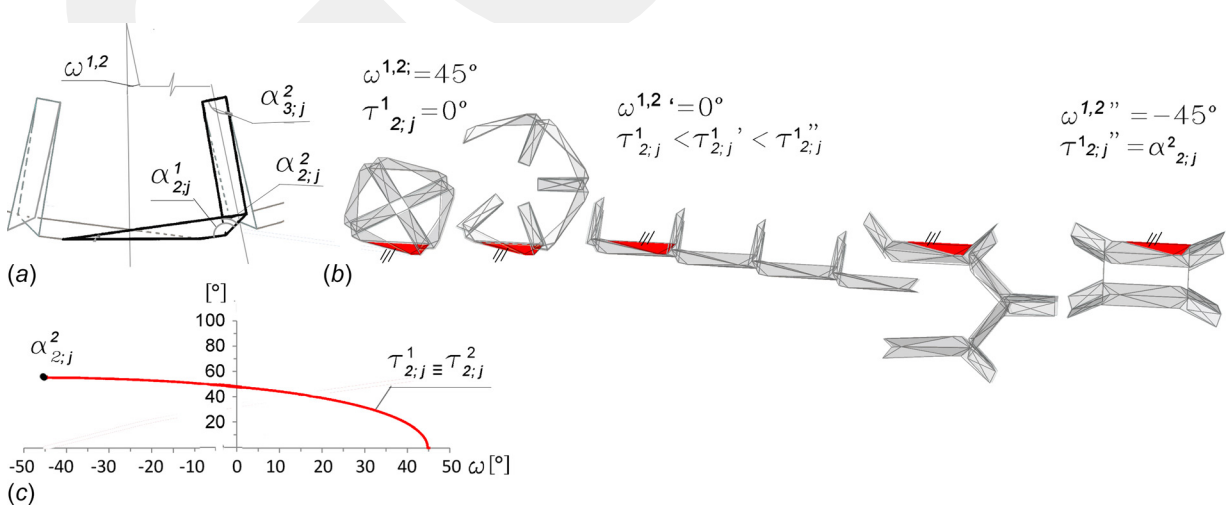

Fig. 6 A mechanism whose planar angles within the double symmetrical linkages are in the form $\alpha^s_{i;j} = \pi - \alpha^{s+1}_{i;j}$: (*a*) one module, (*b*) folding phases, and (*c*) variation of transversal angle $\tau^s_{i;j} \equiv \tau^{s+1}_{i;j}$ between plates at the mixed linkage as a function of the input degree of curvature $\omega^{s,s+1}$

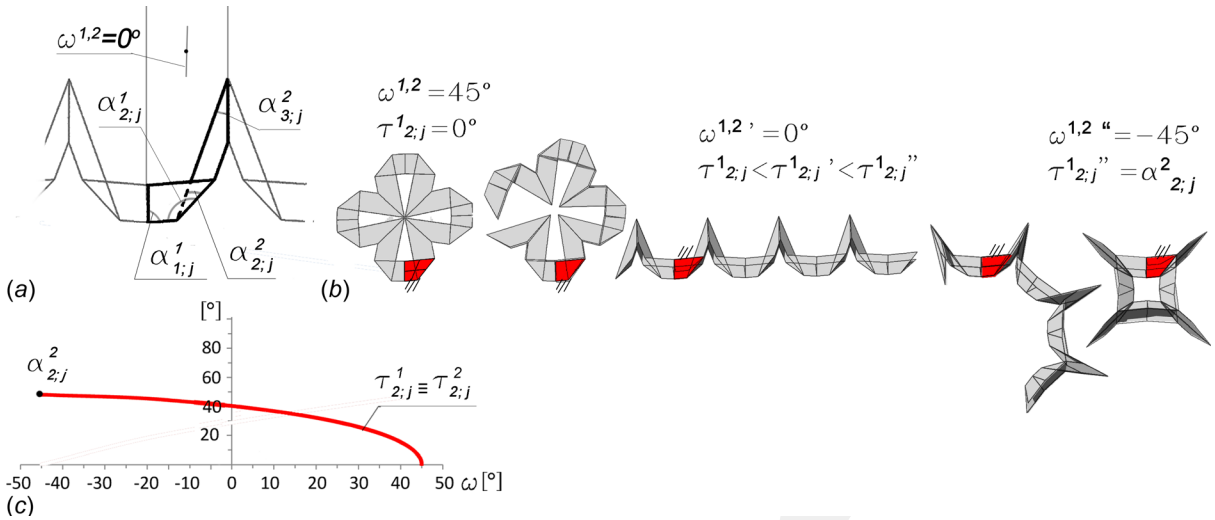

Fig. 7 A mechanism whose planar angles within the double symmetrical linkages are in the form $\alpha^{s}_{i;j} = \alpha^{s+1}_{i;j}$: (*a*) one module, (*b*) folding phases, and (*c*) variation of transversal angle $\tau^{s}_{i;j} \equiv \tau^{s+1}_{i;j}$ between plates at the mixed linkage as a function of the input degree of curvature $\omega^{s,s+1}$

a perpendicular angle $\tau^{s}_{i;j} < (\tau^{s}_{i;j})' < (\tau^{s}_{i;j})''$ into the system of Eqs. (6)–(10), expressed for all the three configurations. The fully flat-folded position is expressed by $\tau^{s}_{i;j} = 0\,\text{deg}, \forall i, j, s$, while the partially flat-folded position is expressed by $(\tau^{s}_{i;j})'' = \alpha^{s+1}_{i;j}$ if $\sin(\alpha^{s}_{i;j}) > \sin(\alpha^{s+1}_{i;j})\tau^{s\prime\prime}_{i;j} = \alpha^{s}_{i;j}$ if $\sin(\alpha^{s}_{i;j}) < \sin(\alpha^{s+1}_{i;j})$. Where assemblies are concerned, the systems are integrated with the constraints already expressed by Eqs. (3) and (4).

3.2 Examples of Transformable–Foldable Ribs Made by Equal Modules. There is no limit to the range of curvatures that the mechanism can reach while folding. Figures 6–8 show three extreme cases where the slope totally reverses, varying between ±45 deg within each equal module. In order to evaluate the role of the spherical links within the mixed linkage connecting two adjacent modules $s;t$ and $s+1;t$, each of the proposed designs uses just two different modules. Furthermore, each module is composed of just one kind of plate so that the correspondent sides of the plates within the module have equal linear length and angles $\omega^{s,s+1}$ and $o^{s,s+1;t}$ have the same value. Figure 6 illustrates a case where the doubly symmetrical spherical linkages are obtained with planar angles at each vertex in the form $\alpha^{s}_{i;j} = \pi - \alpha^{s+1}_{i;j}$, while the other two pictures illustrate the case $\alpha^{s}_{i;j} = \alpha^{s+1}_{i;j}$. The different values of the planar angles produce quite different esthetics and give an example of the formal possibilities offered by the mechanism. Meanwhile, Figs. 6(*c*) to 8(*c*) show the variation of the transversal angle $\tau^{s}_{i;j} \equiv \tau^{s+1}_{i;j}$ between plates at the mixed linkage as a function of the input slope $\omega^{s,s+1}$. The more the spherical lengths of links within the mixed linkage are different, as well as the sine of the correspondent planar angles $\alpha^{s}_{i;j}$ and $\alpha^{s+1}_{i;j}$, the more the mechanism folds smoothly, Figs. 6 and 7. Meanwhile, closer values of the length of the spherical links make the mechanism fold more unevenly, Fig. 8. This result is in harmony with Eqs. (7) and (10).

3.3 Further Examples of Transformable–Foldable Ribs. This section illustrates the three possible, kinematically interchangeable ways to combine different modules. Figures 9–11

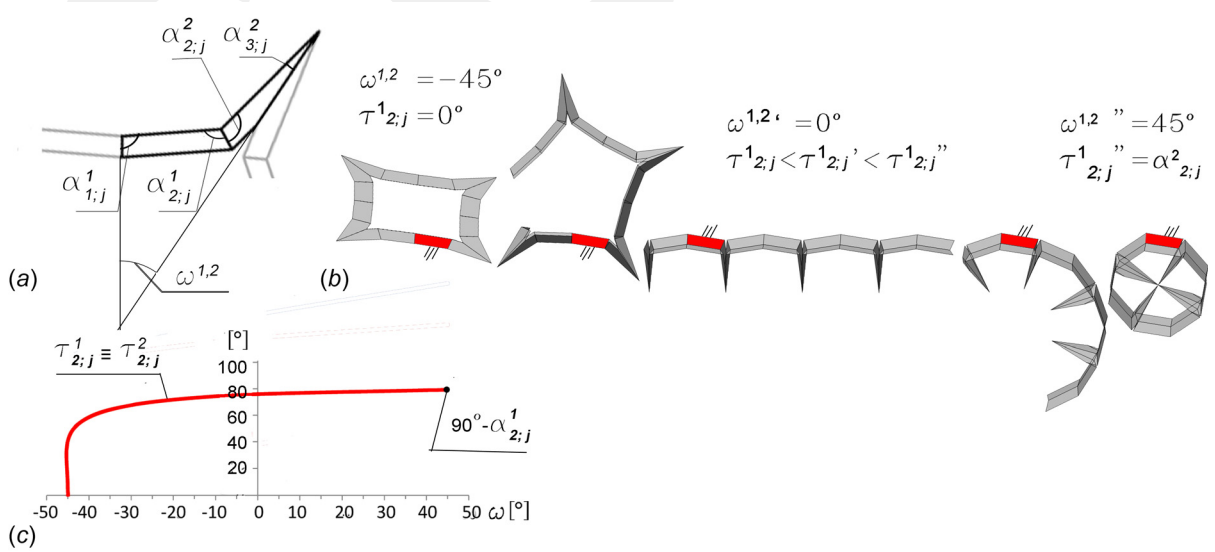

Fig. 8 Another mechanism whose planar angles within the double symmetrical linkages are in the form $\alpha^{s}_{i;j} = \alpha^{s+1}_{i;j}$: (*a*) one module, (*b*) folding phases, and (*c*) variation of transversal angle $\tau^{s}_{i;j} \equiv \tau^{s+1}_{i;j}$ between plates at the mixed linkage as a function of the input degree of curvature $\omega^{s,s+1}$

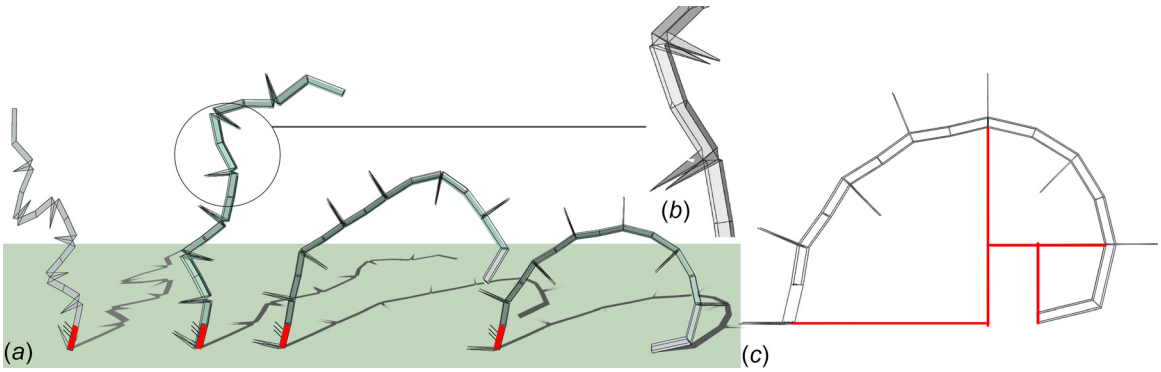

Fig. 9 A folding spiral. The spherical length of links within the quad-based doubly symmetrical linkages changes throughout the assembly in order to fit the variable curvature of the target profiles: (*a*) axonometric views, (*b*) detail, and (*c*) front view at the partially flat-folded state.

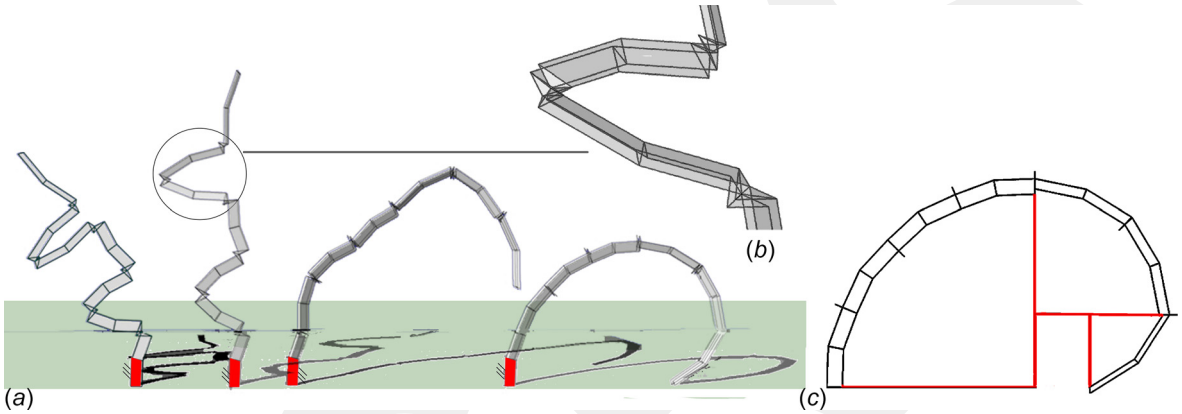

Fig. 10 A folding spiral. The spherical length of links within the mixed linkages changes throughout the assembly in order to fit the variable curvature of the target profiles: (*a*) axonometric views, (*b*) detail, and (*c*) front view at the partially flat-folded state.

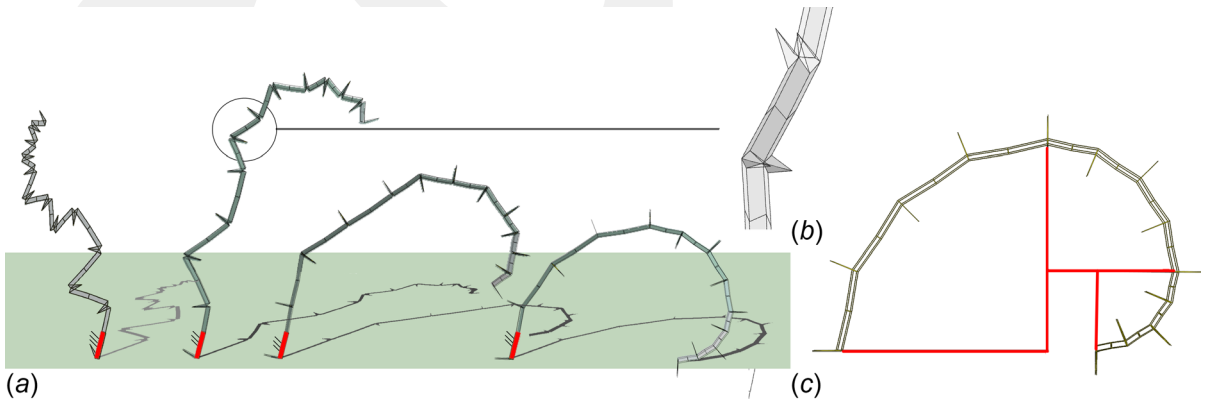

Fig. 11 A folding spiral. The spherical lengths of links are constant throughout, while the linear length of plates changes throughout the assembly in order to fit the variable curvature of the target profiles: (*a*) axonometric views, (*b*) detail, and (*c*) front view at the partially flat-folded state.

illustrate such possibilities applied to the approximation of a Fibonacci spiral. The design's aim was to transform the spiral into a series of longer straight segments, and finally to give it a fully folded state, avoiding self-intersection of the overall mechanism. The models have been tested in Catia@ and developed in a parametric design environment, Grasshopper@ for Rhino@.

In the system depicted in Fig. 9, the spherical length of links within the doubly symmetrical 4*R*-linkages varies from one

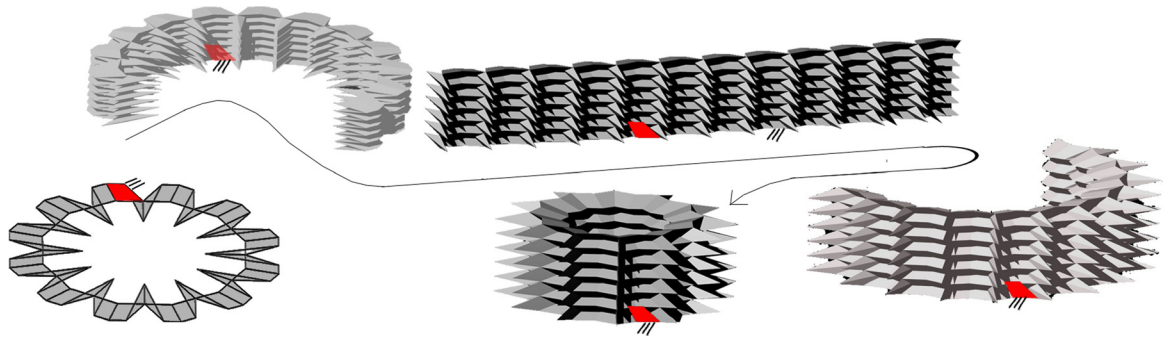

Fig. 12 Folding phases of a surface defined by a circular generatrix and a straight directrix

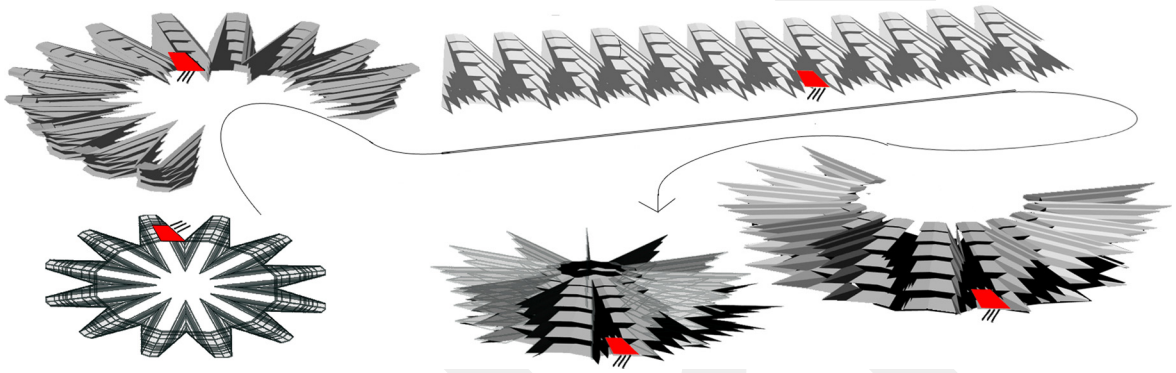

Fig. 13 Folding phases of a surface defined by a circular generatrix and an arched directrix

linkage to the other along the longitudinal direction. This method has been already employed in the assemblies illustrated in Figs. 1–4. There are no constraints that apply to such modifications: the chain of doubly symmetrical 4*R*-linkages keeps folding harmoniously to the flat-folded states.

In the system exemplified in Fig. 10, the target spiral is obtained by varying the spherical length of the mixed linkage according to Eq. (3). It could be pointed out that the linear length of plates within the mixed linkage changes in consequence; although a constant visual depth of the overall mechanism at one desired position can be restored, this modification is not applied here for clarity.

Finally, in the system exemplified in Fig. 11, the spherical image of the modules is actually the same, and so their degree of curvature, $\omega^{s,s+1}$. As detailed in Sec. 4.1, the reference curve is reproduced by varying the length of the approximating polyline and, with it, the linear length of plates and the slope $o^{s,s+1;t}$. Of course, the three methods can be combined.

Looking at any of these examples, it is interesting to note that the very same linkages can point both upward and downward. The variation allows inverting the way of rotation and it is obtained by shifting spherical links $a^s_{i;j}$ and $a^s_{i;j+1}$ within the single module. This change does not create new, different linkages because the two shifted planar angles at that position are supplementary, which means that the spherical length is constant, Eq. (4).

3.4 Examples of Transformable–Foldable Surfaces. According to the constraints, modules can be freely assembled into surfaces until they have the very same spherical image in one direction, i.e., modules are repeated with constant planar angles along that direction. Once designing a desired planar rib, two options arise. The first possibility is to approximate a straight line transversally adding the very same plates. In this case, both the slope $o^{s;t,t+1}$ and the degree of curvature $\omega^{s;t,t+1}$ are null. The derived surface is straight in the transversal direction, Fig. 12. The second option is to approximate a desired transversal curve by adding plates with constant planar angles but variable transversal linear length, Fig. 13. In this way, the slope $o^{s;t,t+1}$ changes along j; it is $\omega^{s;t,t+1} = 0\,\text{deg} \neq o^{s;t,t+1}$. In the picture, a surface with spherical inside ceiling is obtained. The method of approximating the curve is conceptually similar to what is illustrated in Fig. 11, and detailed in Ref. [23] with reference to simple foldable plate structures. With this method, the mechanism can approximate curvilinear grids whose generatrix can be a desired planar curve.

4 Dimensioning the Plates

One should have noticed that the linear length of plates has not been detailed until now. Indeed, spherical linkages are scale-independent. However, a brief introduction to dimensioning is worthwhile to fully understand the proposed illustrative examples and generally the capability and constraints of the plate mechanism. Far from being exhaustive, this section presents the related issues, leaving full discussion to a successive paper oriented toward implementation.

4.1 From Transformable Linkages to Transformable Curves. Under a design perspective, setting not only the slope but also the span of modules allows reproducing desired curves.

As implicit in the definition of foldable mechanisms, the span covered by each module changes with time as a function of the angles between links, here expressed by $\vartheta_{i+1;j}$ and $\tau_{i+1;j}$. However, one may recall that the mechanism is composed of two kinds of modules, which alternate to each other along the j direction and whose dihedral angles at the same instant are different. With an added degree of complexity compared to simply foldable

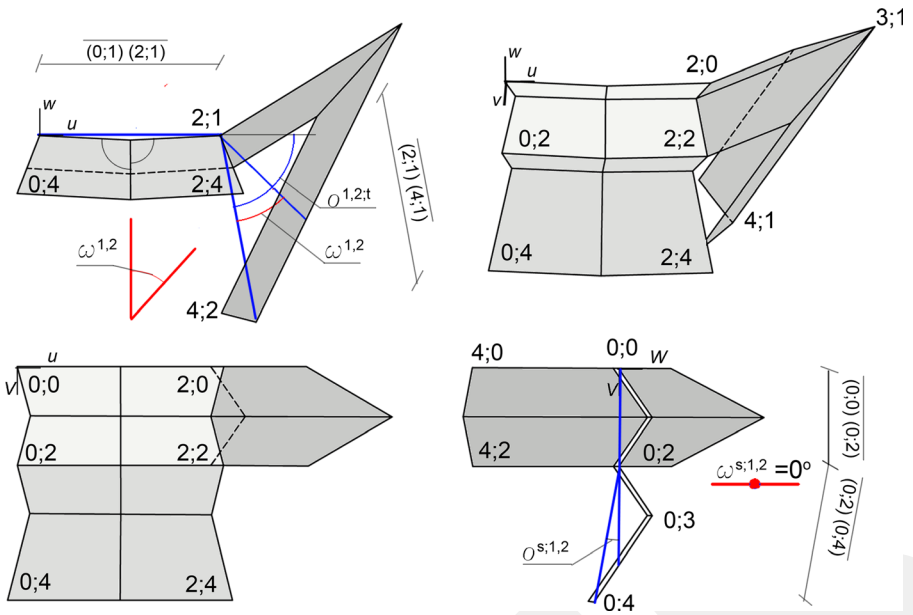

Fig. 14 A plate structure composed by three modules, two of which are composed by plates of different linear length; degrees of curvature $\omega^{s,s+1}$ and $\omega^{s;t,t+1} = 0$ deg; inclination angles $o^{s,s+1;t}$ and $o^{s;t,t+1}$

mechanisms, the proposed system can approximate two desired curves. Assuming links of zero thickness, at the partially folded configuration, one every two modules has zero span and the curve is approximated by half the modules. Meanwhile, in the second desired position, the total number of modules contributes reproducing the target curve. In the examples of Figs. 6 and 7, first the desired span in the partially folded position C'' has been achieved by setting the linear length of half the number of modules; eventually, the linear lengths of previously flat-folded modules have been set so that, in the fully folded position C, opposite plates touch each other. Vice versa, in the example illustrated in Fig. 8, opposite plates touch in the partially folded position C'', and the lengths of the two kinds of plates have been optimized at once. On the contrary, as illustrated in Fig. 13, along the transversal direction i, spherical links are simply translated and just one target curve can be approximated by carrying the linear dimension of plates.

With reference to Fig. 14, the span is related to the linear lengths of plates. Applying the cosine rule, the span in the two directions of a module $s;t$ diagonally defined from vertex $(i_0; j_0)$ to $(i_0+2; j_0+2)$ reads

$$\begin{aligned}\overline{(i_0;j_0)(i_0+2;j_0)} &= \Big((2\overline{(i_0;j_0)(i_0+1;j_0)}\sin\vartheta^{s}_{i_0+1;j_0})^2 \\ &+ (\overline{(i_0;j_0)(i_0+1;j_0)} - \overline{(i+1_0;j_0)(i_0+2;j_0)})^2 \\ &+2\overline{(i_0;j_0)(i_0+1;j_0)}(\overline{(i_0;j_0)(i_0+1;j_0)} \\ &- \overline{(i_0+1;j_0)(i_0+2;j_0)})\sin\vartheta^{s}_{i_0+1;j_0}\Big)^{1/2}\end{aligned} \tag{11a}$$

$$\begin{aligned}\overline{(i_0;j_0)(i_0;j_0+2)} &= \Big((2\overline{(i_0;j_0)(i_0;j_0+1)}\sin\tau^{s}_{i_0;j_0})^2 \\ &+ (\overline{(i_0;j_0)(i_0;j_0+1)} - \overline{(i_0;j_0+1)(i_0;j_0+2)})^2 \\ &+2\overline{(i_0;j_0)(i;j+1)}(\overline{(i_0;j_0)(i_0;j_0+1)} \\ &- \overline{(i_0;j_0+1)(i_0;j_0+2)})\sin\tau^{s}_{i_0;j_0}\Big)^{1/2}\end{aligned} \tag{11b}$$

If plates within each module are symmetrical, i.e., if they have same linear length in addition to same planar angles, Eq. (11) reduces to

$$\overline{(i_0;j_0)(i_0+2,j)} = 2\overline{(i_0;j_0)(i_0+1;j_0)}\sin\vartheta^{s}_{i_0+1;j_0} \tag{12a}$$

$$\overline{(i_0;j_0)(i_0;j_0+2)} = 2\overline{(i_0;j_0)(i_0;j_0+1)}\sin\tau^{s}_{i_0;j_0+1} \tag{12b}$$

The slope over module $s;t$ of a module $s+1;\ t$ diagonally defined from vertex $(i_0+2; j_0)$ *to* $(i_0+4; j_0+2)$ reads

$$\begin{aligned}&o^{s,s+1;t} \\ &= \omega^{s,s+1} \\ &+ \frac{\cos\left(\vartheta^{s+1}_{i_0+3;j}\right)\left(\overline{(i_0+2;j_0)(i_0+3;j_0)} - \overline{(i_0+3;j_0)(i_0+4;j_0)}\right)}{\overline{(i_0+2;j_0)(i_0+4;j_0)}}\end{aligned} \tag{13a}$$

$$o^{s;t,t+1} = \frac{\cos\left(\tau^{s+1}_{i;j}\right)\left(\overline{(i;j)(i;j+1)} - \overline{(i;j+1)(i;j+2)}\right)}{\overline{(i;j)(i;j+2)}} \tag{13b}$$

where $\omega^{s,s+1}$ is formulated according to Eq. (6). If plates within each module have equal linear length, then

$$\omega^{s,s+1} = o^{s,s+1;t} \tag{14a}$$

$$\omega^{s;t,t+1} = o^{s/t,t+1} = 0\,\text{deg} \tag{14b}$$

and Eq. (13*a*) reduces to Eq. (6).

Concerning the parameterization method, the source data to be extracted from the curve is the span and reciprocal slope of consecutive secants traced along the curve. The length of the secants may be set to be constant, to increase with decreasing curvature, to subtend a constant angle, etc. One may refer to the examples in literature based on one's own design intention. Figures 9 and 10 show spirals parameterized in terms of constant arc length, while Fig. 11 shows a spiral where inclination angles are constants and the length of chords varies. It should be noted that constant angles, and thus constant spherical links, are a kinematic constraint along the transversal direction according to Eq. (4). Meanwhile, it is optional along the longitudinal direction. Here, keeping angles constant between as many modules as possible reduces the

computational effort because, if the angles of inclination between modules are the same, then the same geometrical parameters derived by the kinematic constraints, Sec. 3.1, can be applied to all the modules. However, this is a small benefit compared to all the aesthetical, structural, and technological considerations, which affect the evaluation of the numbers and dimensions of plates.

4.2 From Links in the Unit Sphere to Plates. While the motion of spherical linkages can be generally studied on the unit sphere, assigning dimensions to plates may lead to unexpected results. It may happen that some combinations of lengths result in being impracticable because plates intersect with each other during motion, while systems where a side length of plates is progressively reduced to zero, obtaining triangular plates, may have mobility higher than one. Concerning the first issue, if their planar angles are acute and the curvature is particularly high, even plates belonging to adjacent modules can intersect. Locally, the problem may be addressed by changing either the value of some input variables or the linear length of plates. In Ref. [24], a similar problem has been solved by locally changing the shape of plates and in Ref. [25] by adding linkages with the function of "spacers" in between otherwise interfering plates. Where assemblies are concerned, assuming that the polyline traced by the modules is injective, still more distant plates in a row may intersect depending on the relative dimension of them and of all the in-between modules at each folding phase. In the examples proposed in Figs. 9–11, absence of overall self-intersection had been guaranteed by alternatively inverting the direction of folding. Indeed, in so doing, each module folds in respect to the adjacent ones like a panel in a concertina. However, it should be remarked that all these solutions alter the reciprocal slope of modules outside from the fully unfolded configuration. The general case where all the configurations are of concern requires to set optimization criteria and to iteratively apply the same solutions adopted to solve local self-intersection and may be established. However, the criteria, which define the minimal detrimental effects of the desired overall designs, depend on the specific design itself; therefore, addressing the problem exhaustively is out of the scope of this paper.

The situation where triangular plates are used may instead affect mobility. Following Ref. [26], any continuous assembly of quad plates has mobility one by construction. Let us isolate two consecutive vertexes on such generic assembly, Fig. 15(*a*). While each link is defined by three rotational parameters, when assembled, each revolute joint between them removes two rotation parameters. If one considers the four links around vertex 1;1, eight of their twelve rotation parameters are removed by the joints, while fixing one link to the ground further removes three parameters. As one may expect, the 4*R*-linkage has mobility one. The adjacent linkage centered in 1;2 shares with it two links; thus six of its originally free twelve rotational parameters are given. The total of three joints with and between its other two links further remove exactly six parameters so that the motion of this second linkage is fully defined once given the motion of the previous one. One may keep adding linkages and find the same situation between the previous and the last linkages. Indeed, since by construction each linkage shares two links with each adjacent one, all the free motion parameters of the added plates are removed and mobility is kept equal to one [27].

More interesting situations are the degenerate cases where plates have zero linear lengths. Excluding plates reduced to lines or points, even triangular plates actually can create linkages with more than four links. Despite mobility of highly over constrained linkages is a research topics of its own [27–29], the topology of the proposed system is highly repetitive, and a simplified formulation can be developed. The previous mobility condition should be expressed in a generic form: mobility is equal to one until at any inner vertex all plates except up to two are part of a continuous two-plates wide strip whose motion parameters are fully defined. In such case, indeed, one comes back to the situation of a closed chain where some parameters are given by adjacent chains, while the remaining six rotational parameters are fully defined by the joints with and between the two links. As an example, the movement of the first group of hatched plates on the left in Fig. 15(*b*) is fully defined by a common rotational parameter. While there are vertexes where more than four plates meet, the same plates are also part of 4*R*-linkages because of their symmetrical arrangement. The same holds for the triangular plates depicted in Fig. 4. Meanwhile, setting the rotation of four joints in the second hatched area extends the condition expressed above to all this second area, which becomes now fully defined. Similarly, each successive group of plates represented with different color becomes fully defined once four of its rotational parameters are set in addition to the previous ones. While this number is definite for the given topology of the mechanism, in general, different sets of rotational parameters can be selected. In the picture, the joints required to restore mobility one, highlighted, are selected along the boundary. In fact, given the longitudinal symmetry within each module, 4*R*-linkages form by construction around inner vertexes. Therefore, if one is interested in knowing the exact degree-of-freedom of a generic assembly whose vertexes are as usual *i*, *j*, *i* varying from *a* to *b* and *j* from *c* to *d* so that vertexes *a*;*c*, *a*;*d*, *b*;*c,* and *b*;*d* are at the corners of the external boundary; this can be computed considering just a two-plates wide boundary strip, Fig. 15(*c*).

It is

$$M = 1 + \sum_{i=a+1}^{b-1} \left(\left(\frac{p_{i;j=c+1}}{2} - 2 \right) + \left(\frac{p_{i;j=d-1}}{2} - 2 \right) \right) + \sum_{i=a}^{b} \left(\left(\frac{p_{i;j=c}}{2} - 1 \right) + \left(\frac{p_{i;j=d-1}}{2} - 1 \right) \right) \tag{15}$$

where M is the mobility of the mechanism' and $p_{i;j}$ is the number of plates around vertex i, j.

Considering the overall two-plates wide boundary of the surface would allow extending the formula to the extreme case where all plates are triangular. However, in such cases, mobility will always be higher than one.

Finally, while equal linkages on the unit sphere are coincident, in practical applications, a high number of linkages require special care when setting the input link, even if mobility is equal to one. Interesting studies on the relationships between the position and direction of symmetrical forces and symmetry-based linkages have been proposed in Ref. [29].

5 Conclusion

A novel, modular foldable plate mechanism had been presented. The mechanism, first in its field, has transformational capabilities since the slope of each module over the adjacent one can vary not only in magnitude but also in sign. In analogy with planar linkages, the Grashof's criterion has been used to demonstrate the role of symmetry in the folding range of the mechanism.

The particular behavior of the proposed mechanisms is based on the interposition of a 4*R*-linkage having one line of symmetry between doubly symmetrical 4*R*-linkages. Its unequal links break the transmission of even dihedral angles between the adjoined linkages; they force the linkages on one side to become collinear while the ones on the other side are still unfolded. Meanwhile, since all linkages in the row share at least one common line of symmetry, the mechanism is capable of folding flat in the plane containing that line.

The dimensional synthesis for three target positions has been illustrated in Sec. 3. There is no limit to the range of curvatures that the mechanism can achieve while folding. Specifically, each module can reach three desired slopes over the adjacent one during motion, as exemplified in Sec. 3.2; eventually, other different

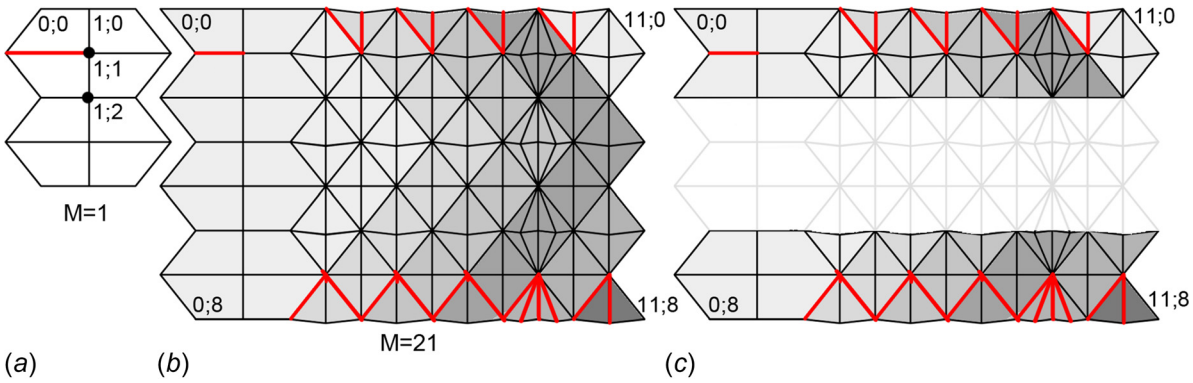

Fig. 15 (*a*) Any assembly of quad plates has mobility one. A possible input joint is highlighted. (*b*) An assembly composed by triangular and quadrangular plates. Highlighted joints are in the necessary number and possible position to achieve a mechanism with mobility one. Moving from left to right, and setting the selected joints, the hatched areas become fully defined. (*c*) The mobility of an assembly composed by triangular and quadrangular plates can be studied focusing on the border longitudinal strips of plates.

modules can be combined in order to obtain curves whose shape changes over time, Sec. 3.3. Equal ribs can be added along the perpendicular direction in order to create surfaces of translation with a straight directrix. In case the directrix is not straight, the transversal span of the obtained surface changes during folding. The surface is also very sharp, which may make it unusable in many applications. Since the mechanism is highly overconstrained, the problem may be solved through the removal of the most pointed plates.

Setting the span of modules allows approximating two desired curves. Since the linear length of plates does not affect the kinematic behavior of the spherical linkages, one may freely vary the linear dimensions and test their formal results. In the symmetrical curves proposed in Figs. 5–7, the linear length of plates is such that, in the fully folded configurations, opposite plates touch each other. Meanwhile, each of the three spiral shapes approximated in Figs. 9–11, which are formally equal, achieves a different shape in the fully folded configuration. These design explorations have been performed in real time in a parametric design environment, Grasshopper@ for Rhino@. However, for more rigorous applications, further studies are needed in order to develop an optimization method, which allows avoiding interference of plates with minimal detachment from the shape to be approximated, Sec. 4.1. Another issue which cannot be directly addressed in the parametric environment is mobility. Until quadrangular plates are used, mobility is equal to one. However, if a side of plates is reduced to zero length, then mobility may increase because vertexes of the triangular plates become centers of linkages composed by more than four links. Such possibility is discussed in Sec. 4.2.

The capability of the proposed mechanism to substantially change its shape may open new areas of application. A successive theoretical development will be to further test the design possibilities offered by the uneven folding of different linkages, extending symmetry from the organization of the single module to the overall composition of modules. It is known that particular symmetrical 3D arrangements of the overall modular structure have mobility one and both transformable polyhedrons composed by 3D bodies [30] and scalable polyhedrons composed of planar links [31] have been proposed in literature. Similarly, the proposed system may be further studied in order to create 3D intertwine with mobility one.

References

[1] Chen, Y., Feng, J., and Fan, L., 2013, "Mobility and Kinematic Simulations of Cyclically Symmetric Deployable Truss Structures," Proc. Inst. Mech. Eng., Part C, **227**(10), pp. 2218–2227.

[2] Mitani, J., 2009, "A Design Method for 3D Origami Based on Rotational Sweep," Comput.-Aided Des. Appl., **6**(1), pp. 69–79.

[3] Kokotsakis, A., 1933, "Über Bewegliche Polyeder," Math. Ann., **107**(1), pp. 627–647.

[4] Izmestiev, I., 2017, "Classification of Flexible Kokotsakis Polyhedra With Quadrangular Base," Int. Math. Res. Not., **2017**(3), pp. 715–808.

[5] Stachel, H., 2010, "A Kinematic Approach to Kokotsakis Meshes," Comput. Aided Geom. Des., **27**(6), pp. 428–437.

[6] Xie, R., Chen, Y., and Gattas, J. M., 2015, "Parametrisation and Application of Cube and Eggbox-Type Folded Geometries," Int. J. Space Struct., **30**(2), pp. 99–111.

[7] Schenk, M., and Guest, S. D., 2013, "Geometry of Miura-Folded Metamaterials," Proc. Natl. Acad. Sci., **110**(9), pp. 3276–3281.

[8] Sareh, P., and Guest, S. D., 2015, "Design of Isomorphic Symmetric Descendants of the Miura-ori," Smart Mater. Struct., **24**(8), p. 085001.

[9] Watanabe, N., and Kawaguchi, K., 2009, "The Method for Judging Rigid Foldability," Fourth International Conference on Origami in Science, Mathematics, and Education (4OSME), Pasadena, CA, Sept. 8–10.

[10] Tachi, T., 2009, "Simulation of Rigid Origami," Fourth International Conference on Origami in Science, Mathematics, and Education (4OSME), Pasadena, CA, Sept. 8–10.

[11] Tachi, T., 2009, "3D Origami Design Based on Tucking Molecule," Fourth International Conference on Origami in Science, Mathematics, and Education (4OSME), Pasadena, CA, Sept. 8–10.

[12] Yasuda, H., Chen, Z., and Yang, J., 2016, "Multitransformable Leaf-Out Origami With Bistable Behavior," ASME J. Mech. Rob., **8**(3), p. 031013.

[13] Resch, R. D., 1973, "The Topological Design of Sculptural and Architectural Systems," National Computer Conference and Exposition (AFIPS), New York, June 4–8, pp. 643–650.

[14] Guest, S., and Pellegrino, S., 1994, "The Folding of Triangulated Cylinders—Part I: Geometric Considerations," ASME J. Appl. Mech., **61**(4), pp. 773–777.

[15] Evans, T. A., Lang, R., Magleby, S.P., and Howell, L. L., 2015, "Rigidly Foldable Origami Gadgets and Tessellations," R. Soc. Open Sci., **2**(9), p. 150067.

[16] Chiang, C. H., 1988, *Kinematics of Spherical Mechanisms*, Cambridge University Press, Cambridge, UK.

[17] Gosselin, C. M., and Angeles, J., 1990, "Singularity Analysis of Closed-Loop Kinematic Chains," IEEE Trans. Rob. Autom., **6**(3), pp. 281–290.

[18] Huffman, D. A., 1976, "Curvature and Creases: A Primer on Paper," IEEE Trans. Comput., **C-25**(10), pp. 1010–1019.

[19] Barreto, P. T., 1997, "Lines Meeting on a Surface: The Mars Paperfolding," Origami Science and Art: Second International Meeting of Origami Science and Scientific Origami, OSME, Otsu, Japan, Nov. 29–Dec. 2, pp. 343–359.

[20] Beatini, V., 2015, "Polar Method to Design Foldable Plate Structures," J. IASS, **56**(2), pp. 125–136.

[21] Gioia, F., Dureisseix, D., Motro, R., and Maurin, B., 2012, "Design and Analysis of a Foldable/Unfoldable Corrugated Architectural Curved Envelop," ASME J. Mech. Des., **134**(3), p. 031003.

[22] Gattas, J. M., Wu, W., and You, Z., 2015, "Miura-Base Rigid Origami. Parameterizations of First-Level Derivative and Piecewise Geometries," ASME J. Mech. Des., **135**(11), p. 111011.

[23] Beatini, V., 2015, "Translational Method for Designing Folded Plate Structures," Int. J. Space Struct., **30**(2), pp. 85–99.

[24] Zhang, Y., Gao, W., Paredes, L., and Ramani, K., 2016, "CardBoardiZer. Creatively Customize, Articulate and Fold 3D Mesh Models," Conference on Human Factors in Computing Systems (CHI), Santa Clara, CA, May 7–12, pp. 897–907.

[25] Hoberman, C., 1991, "Reversibly Expandable Structures," U.S. Patent No. 4981732 A.

[26] Beatini, V., and Korkmaz, K., 2014, "Shapes of Miura Mesh Mechanism With Mobility One," Int. J. Space Struct., **28**(2), pp. 101–115.
[27] Chen, Y., Feng, J., and Liu, Y., 2016, "A Group-Theoretic Approach to the Mobility and Kinematic of Symmetric Over-Constrained Structures," Mech. Mach. Theory, **105**, pp. 91–107.
[28] Pellegrino, S., and Calladine, C. R., 1986, "Matrix Analysis of Statically and Kinematically Indeterminate Frameworks," Int. J. Solids Struct., **22**(4), pp. 409–428.
[29] Chen, Y., and Feng, J., 2015, "Mobility of Symmetric Deployable Structures Subjected to External Loads," Mech. Mach. Theory, **93**, pp. 98–111.
[30] Gao, W., Ramani, K., Cipra, R. J., and Siegmund, T., 2013, "Kinetogami: A Reconfigurable and Printable Sheet Folding," ASME J. Mech. Des., **135**(11), p. 111009.
[31] Kiper, G., and Söylemez, E., 2013, "Polyhedral Linkages Obtained as Assemblies of Planar Link Groups," Front. Mech. Eng., **8**(1), pp. 3–9.